A Change of Perspective on Single- and Double-Stage Optical PMD Compensation

Armando Vannucci, *Member, IEEE*, and Alberto Bononi

***Abstract*—We present a rigorous investigation on how to optimize the degrees of freedom of optical polarization mode dispersion (PMD) compensators composed of differential group delay sections and polarization controllers, up to two stages. The analytical treatment relies on the *extracted Jones matrices* of the transmission and compensation fibers. The analysis of a single-stage compensator with two degrees of freedom (fixed DGD) is based on the maximization of the eye opening, as provided by the *generalized Chen formula*. The outage probability is quantified through a fast semi-analytical technique. It is shown how the benefits of single-stage compensation are strongly reduced and can lead to outage events, when certain critical input states of polarization are launched into transmission fibers with strong eigenmodes depolarization (i.e., strong higher order PMD). Focusing on such transmission fibers and input configurations, a novel algorithm is introduced for controlling a double-stage compensator with five degrees of freedom. The algorithm is based on an ideal equalization of the transmission fiber at half the bit-rate, realized resorting to spherical geometry. To this aim, we show that the first compensator stage must be a PMF fiber with very large DGD, equal to the bit period, in order to compensate the most critical configurations associated with outage events.**

***Index Terms*—Extracted Jones matrices, polarization mode dispersion (PMD), PMD compensation.**

I. Introduction

POLARIZATION mode disperison (PMD) in the last 15 years has deserved a great deal of attention, both from industrial and academic research communities. The intellectual challenge and the strategic importance of this topic have increased along with the increasing Sonet/SDH hierarchy levels under consideration, evetually becoming the limiting factor for the deployment of 40-Gb/s systems on installed fibers. The ups and downs of the photonics market have influenced to a large extent the efforts devoted to this strategic problem. Looking at the scientific literature today, it luckily seems that most of such efforts are behind our shoulders. Polarization in fiber optics poses a number of questions, among which: modeling, statistical analysis, interactions with group velocity dispersion, Kerr nonlinearities, optical amplification, and polarization dependent loss. From a systems engineer's perspective, PMD compensation is the principal challenge.

Manuscript received October 9, 2007; revised February 7, 2008. Published August 29, 2008 (projected). This work was supported in part by Alcatel under research contract URP/01.01.

The authors are with the Università di Parma, Dipartimento di Ingegneria dell'Informazione, Parma I-43100, Italy.

Color versions of one or more of the figures in this paper are available online at http://ieeexplore.ieee.org.

Digital Object Identifier 10.1109/JLT.2008.920537

Different methods are envisaged for contrasting PMD, ranging from *passive* methods, employing forward error correction codes and robust modulation formats [1] or posing the rules for fabricating future fibers with minimal PMD impact [2], to *active* methods for compensating the distorted signal in the electrical domain (see, e.g., [3] and citations therein) or in the optical domain, thus avoiding the complication of including the square-law photodetector in the system model. Optical PMD compensators (OPMDC) can be realized by cascading a number of stages, each made by a polarization control part followed by a first-order PMD section [4]. Practical realizations can equivalently resort to discrete elements, as polarization controllers/rotators, polarization maintaining fiber (PMF) sections, and variable differential group delay (DGD) elements, or to planar lightwave circuits (PLC). In particular, confining the attention to single and double-stage OPMDC, a comprehensive analysis of system architectures is provided in [5], where the different solutions and their related performance are associated with the number of degrees of freedom, which quantifies the complexity (and stability) of demanded control algorithms.

The curse of PMD is its stochastic nature; hence, the performance of systems limited by PMD should always be quantified in terms of outage probability (OP), where an outage event is defined as the penalty (eye-closure or sensitivity) exceeding a few dBs. The performance of the different compensator architectures, in terms of tolerable average DGD for a given OP, along with their limits are well assessed in the literature. On the other hand, we believe that a deeper focus on what are the key features of system configurations that make a compensator fail deserve further investigation. Understanding the circumstances that determine outage events provides the rationale for improving the compensator structure and/or controls.

The focus in this paper is thus on the optimization criterion of a single-stage compensator and the analysis of outage events where the compensator fails. This procedure shows the path for a rational extension of the compensator, with minimal increase in complexity, and its related control strategy. Although it is beyond the scope of this paper to analyze the practical solutions that make the control algorithms work effectively, we just mention that tracking of the polarization state of the transmission fiber is necessary in a time-varying scenario and, hence, proper devices for monitoring the system state and feed control signals back to the compensator stages are demanded. Recent solutions using silica planar waveguides [6] have been proposed for monitoring the state of polarization (SOP) as a function of frequency across a modulated signal spectrum, with high speed and resolution. Such devices, complemented by a proper control logic, can be flexibly adapted to the estimation of channel parameters needed by the compensators that we shall discuss.

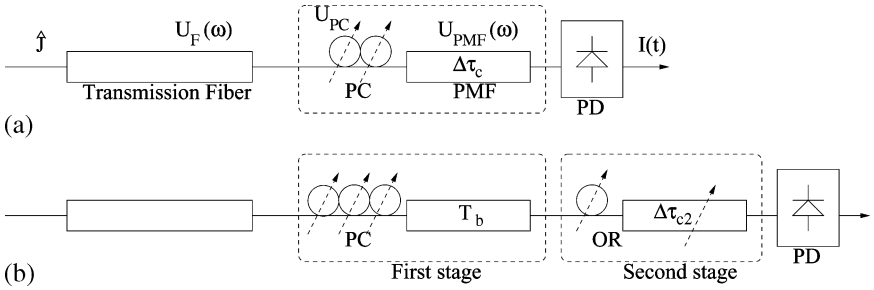

Fig. 1. Principle of operation for: (a) single-stage fixed-DGD optical compensator; (b) double-stage compensator with 5 degrees of freedom. $\hat{J}$ is the Jones input SOP; $U_F(\omega)$ and $U_{\rm PMF}(\omega)$ the transmission and compensation fiber Jones matrices. PC = Polarization Controller; OR = Optical Rotator; PD = Photodiode.

The paper is organized as follows. In Section II-A, we discuss the optimization of a single-stage OPMDC with two degrees of freedom, which maximizes the eye opening. To this aim, we first review the formalism of extracted matrices, the Pauli vectors chain rule and the Generalized Chen Formula, as basic notions needed to cast the problem. The performance of the single-stage compensator driven by the described algorithm is quantified and discussed in Sections II-B and II-C, highlighting the physical limits of such compensator in relation with critical configurations of the transmission fiber and input SOP. In Section III-A, we describe a control algorithm for a double-stage OPMDC, with five degrees of freedom, able to overcome the limits discussed above. The optimization criterion will be the ideal equalization of the transmission matrix at two opposite frequencies. Such a goal is achieved resorting to spherical geometry, which shows that the DGD of the first stage should be as large as the bit period T_b. In Section III-B, the benefits of the double-stage compensator are quantified, showing how inverting the Jones matrix at two *edge* frequencies effectively equalizes the transmission fiber on the whole signal bandwidth. In both Sections II-B and III-B, the OP is quantified through a semi-analytical technique based on the Sensitivity Penalty obtained by simulating transmission on a pool of fiber samples emulated with the Random Waveplate Model (RWM) with 100 plates. Such fibers were selected by running a Multicanonical Monte Carlo algorithm [7] so as to find samples whose first- and second-order PMD vectors magnitude $(|\vec{\Omega}|, |\vec{\Omega}_\omega|)$ cover configurations with probability down to 10^{-25}.

The following notation is adopted throughout the paper: Jones and Müller matrices are denoted by capital letters, as well as (2 $\times$ 1) complex Jones vector, while (3 $\times$ 1) real Stokes vectors are denoted by lower-case letters. All vectors are denoted by an arrow and unit magnitude vectors by an hat, except for 4-D Pauli vectors, which are underlined. A column vector with elements a,b, c is expressed as $[a; b; c]$. The symbols $\cdot$ and $\times$ denote vector scalar and cross product, ^{T} deontes matrix transpose and † the adjoint matrix, i.e., transpose-conjugate. The zero-th Pauli matrix σ_0 is the (2 $\times$ 2) identity matrix while I is the (3 $\times$ 3) identity matrix.

II. Single-Stage Compensator With Fixed DGD

A. Theory

Consider the transmission system depicted in Fig. 1(a). A totally polarized input field, represented by the Jones vector $\vec{E}_{in}(\omega) = E_{in}(\omega)\hat{J}$, with complex envelope $E_{in}(\omega)$ and unit magnitude Stokes SOP $\hat{j}$, is launched into a transmission fiber with Jones matrix $U_F(\omega)$. The OPMDC consists of a polarization controller (PC) followed by a PMF; after photodetection, the output current is $I(t)$. Nelecting all common-mode distorsions, such as group velocity dispersion (GVD) or attenuation, which have an impact only on the scalar input field $E_{in}(\omega)$, the fiber Jones matrix has unit determinant and can be expressed as [8]

$$U_F(\omega) = U_0 U_r(\omega) = U_0 \mathrm{e}^{-\frac{j}{2}\Delta\phi_r(\omega)\left(\hat{b}_r(\omega)\cdot\vec{\sigma}\right)} \tag{1}$$

where $U_0 \triangleq U_F(0)$ is the value at the carrier frequency, while the exponential matrix $U_r(\omega)$ is what we call the *right-extracted Jones matrix* of the fiber [9], with *retardation* $\Delta\phi_r(\omega)$ and unit magnitude *eigenmode* $\hat{b}_r(\omega)$; finally, $\vec{\sigma}$ is the *spin vector*, i.e., a tensor whose three entries are the unitary Pauli matrices $\sigma_{1,2,3}$ [8]. As is well known, such exponential matrix causes a rotation of the input SOP (ISOP), in Stokes space, around the eigenmode by a counterclockwise angle equal to the retardation, for every frequency. Since $\Delta\phi_r(0) = 0$ by definition, as far as the extracted matrix is concerned, a null retardation is applied to a sinusoidal input signal at the carrier frequency and its SOP is left unchanged at the output.

Now, call U_{PC} the frequency-independent Jones matrix of the PC and $U_{\rm PMF}(\omega)$ the unitary Jones matrix of the compensating fiber. Since such fiber is a PMF, with constant DGD $\Delta\tau_c$ and eigenmode $\hat{b}_c$ (in the laboratory frame of reference), the electrical field being photodetected is

$$\begin{aligned}\vec{E}_{\rm out}(\omega) &= E_{in}(\omega)U_{\rm PMF}(\omega)U_{PC}U_0U_r(\omega)\hat{J} \\ &= E_{in}(\omega)U_{PC}U_0\mathrm{e}^{-\frac{j}{2}\Delta\tau_c\omega(\hat{e}_c\cdot\vec{\sigma})}U_r(\omega)\hat{J}\end{aligned} \tag{2}$$

where $\hat{e}_c = M_0^T M_{PC}^T \hat{b}_c$ is the PMF eigenmode *as seen by the input signal*, i.e., rotated by the inverse of the Müller matrix M_{PC} of the polarization controller and M_0 of the fiber at $\omega = 0$. Since the PC provides two degrees of freedom, $\hat{e}_c$ can be brought anywhere on the Poincaré sphere, by controlling the PC in the search for the optimal compensator position. The output photodetected intensity $I(t) = |\vec{E}_{\rm out}(t)|^2$, obtained by inverse-transforming (2), does not depend on the frequency-independent matrix $U_{PC}U_0$ but only on the overall *right-extracted Jones matrix* of the link

$$U_t(\omega) = U_c(\omega)U_r(\omega) = \mathrm{e}^{-\frac{j}{2}\Delta\tau_c\omega(\hat{e}_c\cdot\vec{\sigma})}\mathrm{e}^{-\frac{j}{2}\Delta\phi_r(\omega)\left(\hat{b}_r(\omega)\cdot\vec{\sigma}\right)} \tag{3}$$

where $U_c(\omega) = U_0^\dagger U_{PC}^\dagger U_{\rm PMF}(\omega) U_{PC} U_0 = {\rm e}^{-(i/2)\Delta\tau_c\omega(\hat{e}_c\cdot\vec{\sigma})}$ is the Jones matrix of the compensating PMF subject to the similarity transformation that rotates its eigenmode $\hat{b}_c$ to $\hat{e}_c$.

Extracted matrices have been introduced in [9] as an alternative approach to model PMD (of any order). Knowing the retardation $\Delta\phi_r(\omega)$ and the eigenmode $\hat{b}_r(\omega)$ makes the output field in (2) ready to calculate, without solving the so-called *inverse PMD problem* [10], i.e., the need for finding suitable expression for the Jones matrix once the PMD vector and some of its derivatives are given. This approach is linked to the classical representation in terms of the *PMD vector* $\vec{\Omega}_i(\omega) = \Delta\tau(\omega)\hat{q}_i(\omega)$, where $\Delta\tau$ is the DGD and $\hat{q}_i$ the input principal state of polarization (PSP), by several equalities [9]. At the reference frequency, the frequency derivative of the retardation $\Delta\phi_r'(0) = \Delta\tau(0)$ equals the DGD; the second derivative $\Delta\phi_r''(0) = \Delta\tau'(0)$ equals the polarization-dependent chromatic dispersion (PCD); the eigenmode $\hat{b}_r(0) = \hat{q}_i(0)$ is aligned with the input PSP, but its depolarization, i.e., the motion in frequency, $\vec{b}_r'(0) = \vec{q}_i'(0)/2$ happens in the same direction at half the speed at which the PSPs depolarize. This fact, for which simulation evidence is provided in [9], implies that the extracted eigenmodes, $\hat{b}_r(\omega)$ and its orthogonal, provide a more stable frame of reference for representing PMD than the PSPs, in a neighborhood of the carrier frequency.

The probability distributions and statistical properties of the eigenmodes and retardation of the *un*-extracted Jones matrix of long single mode fibers have been extensively characterized in [11], along with the statistics of the fiber *Pauli vector*

$$\underline{u} = \begin{bmatrix} u_0 \\ \vec{u} \end{bmatrix} = \begin{bmatrix} \cos(\Delta\phi/2) \\ -i\sin(\Delta\phi/2)\hat{b} \end{bmatrix} \Longleftrightarrow U = \underline{u}\cdot\begin{bmatrix} \sigma_0 \\ \vec{\sigma} \end{bmatrix} \quad (4)$$

which provides a compact way of representing a given Jones matrix $U = \exp\{-(i/2)\Delta\phi(\hat{b}\cdot\vec{\sigma})\}$, expanded on the basis of Pauli matrices $\sigma_{0,1,2,3}$, at any given frequency. Pauli vectors provide a convenient tool when two or more Jones matrices are cascaded: in our case, the algebraic chain rule for obtaining the Pauli vector $\underline{u}_t$ of U_t in (3) is [9], [11]

$$\underline{u}_t = \begin{bmatrix} u_{0c} & \vec{u}_c^T \\ \vec{u}_c & u_{0c}I + i[\vec{u}_c\times] \end{bmatrix} \underline{u}_r \quad (5)$$

where $\underline{u}_c(\omega) = [u_{0c}(\omega); \vec{u}_c(\omega)] = [\cos(\Delta\tau_c\omega/2); -i\sin(\Delta\tau_c\omega/2)\hat{e}_c]$ and $\underline{u}_r(\omega) = [u_{0r}(\omega); \vec{u}_r(\omega)] = [\cos(\Delta\phi_r(\omega)/2); -i\sin(\Delta\phi_r(\omega)/2)\hat{b}_r(\omega)]$ are the Pauli vectors of $U_c(\omega)$ and $U_r(\omega)$. The result in (5) recasts in our terminology a well known property in the algebra of quaternions [12], [13].

Based on the Pauli vector of any given fiber link, we have derived in [9] analytic expressions for the ouput intensity where the dependence of $I(t)$ on the ISOP $\hat{j}$ is made explicit. Such an approach has general validity and can include other polarization-dependent system impairments.[1] For our purposes, the main value of an explicit expression for $I(t)$ is that we obtain an analytic expression for the eye opening (EO) Y of the signal received after photodetection and electrical filtering (the electrical filter is not reported in Fig. 1) [9]

$$Y(\omega_0) = \left|\frac{1}{2}\left(\underline{u}_t(\omega_0) + \underline{u}_t^*(-\omega_0)\right)\cdot[1;\hat{j}]\right| = \sqrt{c(\omega_0)^2 + \left(\vec{o}(\omega_0)\cdot\hat{j}\right)^2} \quad (6)$$

where $\omega_0 = \pi/T_b$, T_b being the bit period. The two terms $c(\omega_0) = (1/2)(u_{0t}(\omega_0) + u_{0t}(-\omega_0))$ and $\vec{o}(\omega_0) = (i/2)(\vec{u}_t(\omega_0) - \vec{u}_t(-\omega_0))$ are real and depend on the eigenmode $\hat{b}_t(\pm\omega_0)$ and retardation $\Delta\phi_t(\pm\omega_0)$ of the extracted Jones matrix $U_t(\pm\omega_0)$ of the whole link (transmission fiber plus compensator). The expression in (6) is called *Generalized Chen's formula* (GCF) and is derived under the assumption that the *eye-closing sequence* is 101010..., i.e., that an alternation of marks and zeros is the most critical bit pattern yielding the smallest EO. In order to gain further insight into (6), it can be proven [9] that $Y(\omega)$ is the magnitude of the *small-signal baseband transfer function* $H(\omega)$, linking the input and output intensity of an amplitude-modulated carrier with modulation frequency ω, as derived in [4]. The argument ω_0 in (6) identifies the fundamental frequency of a signal modulated by the 101010... pattern, hence its value $\omega_0 = 2\pi/2T_b$. The accuracy of the GCF is quantified in [9], Sec.5.4, showing that (6) deviates from the actual EO when the eye closure penalty becomes significant. Nonetheless, the compensation strategy pursued here relies only on the gradient of the EO, as seen in the Appendix and further discussed in Section II-C based on numerical results.

It is interesting to note that some PMD compensator control algorithms, namely those based on the *spectral lines* [15], monitor the RF spectrum after photodetection at ω_0 (plus possibly other frequencies). In addition, two common compensation strategies devised for first-order PMD can be interpreted in the light of (6) as follows. From (6), we see that $Y(\omega_0) \le 1$ equals one if either $\Delta\phi_t(\omega_0) = -\Delta\phi_t(-\omega_0) = 0$, i.e., U_t is the identity matrix, at half the modulation frequency, or if the following three conditions are met: i) $\Delta\phi_t(\omega_0) = -\Delta\phi_t(-\omega_0) \neq 0$, i.e., the global retardation is an odd function at ω_0; ii) $\hat{b}_t(\omega_0) = \hat{b}_t(-\omega_0)$, i.e., there is no depolarization of the global eigenmode at $\pm\omega_0$; and iii) $\hat{j}$ is aligned with such a global eigenmode. A sufficient condition for the above conditions to be met is that the global link can be modeled as a PMF, on the signal bandwidth, which imples a linear retardation $\Delta\phi_t(\omega) = \Delta\tau_t\omega$ and frequency independent eigenmode $\hat{b}_t = \hat{q}_{i,t}$ coinciding with the input PSP, hence satisfying conditions i) and ii). Condition iii) then corresponds to the well known *PSP lauch condition* [16], which avoids PMD by controlling the ISOP at the transmitter. As a second example, let us now evaluate $\vec{o}(\omega_0)$ in the limit for $\omega_0 \to 0$: since $\Delta\phi_t$ is the retardation of the global *extracted* Jones matrix, $\Delta\phi_t(\omega_0) \simeq -\Delta\phi_t(-\omega_0)$ tends to zero and $c(\omega_0)$ tends to one, while, exploiting the relationships between eigenmode/retardation and the input PMD vector given above, one can easily demonstrate that $\vec{o}(\omega) \to (\omega/2)\vec{\Omega}_{i,t}(0)$. Hence, to maximize $Y(\omega_0)$, the optimal compensator position is the one that brings the global input PMD vector $\vec{\Omega}_{i,t}$ of the line plus compensator

[1] In [14], a similar expression for $I(t)$ was applied to determine the output RF spectrum of a system with both PMD and PDL.

parallel to the ISOP $\hat{j}$: a compensation strategy that is well known in the literature [17].

Our objective is here to maximize the eye opening, as provided by the GCF, by acting on the PC so as to control the compensator eigenmode $\hat{e}_c$, as seen at the input. Given $U_r(\pm\omega_0)$ and the compensator DGD $\Delta\tau_c$, we first make the dependence of the GCF (6) on the unknown $\hat{e}_c$ explicit. Using the the Pauli vectors chain rule (5), and exploiting the even/odd symmetries of $u_{0c}(\omega)$ and $\vec{u}_c(\omega)$, we get

$$c(\omega_0) = \delta - \vec{a}\cdot\hat{e}_c; \quad \vec{o}(\omega_0)\cdot\hat{j} = \gamma + \vec{b}\cdot\hat{e}_c \tag{7}$$

where we introduced the symbols

$$\begin{aligned}\delta &= \cos\left(\frac{\Delta\tau_c\omega_0}{2}\right)u^e_{0r};\ \gamma = \cos\left(\frac{\Delta\tau_c\omega_0}{2}\right)\hat{j}\cdot\vec{u}^o_r \\ \vec{a} &= \sin\left(\frac{\Delta\tau_c\omega_0}{2}\right)\vec{u}^o_r;\ \vec{b} = \sin\left(\frac{\Delta\tau_c\omega_0}{2}\right)\left(u^e_{0r}\hat{j} + \vec{u}^e_r\times\hat{j}\right)\end{aligned} \tag{8}$$

based on the following definitions:

$$\begin{aligned}u^{e,o}_{0r} &= \frac{1}{2}\left(\cos\left(\frac{\Delta\phi_r(\omega_0)}{2}\right) \pm \cos\left(\frac{\Delta\phi_r(-\omega_0)}{2}\right)\right) \\ \vec{u}^{e,o}_r &= \frac{1}{2}\left(\sin\left(\frac{\Delta\phi_r(\omega_0)}{2}\right)\hat{b}_r(\omega_0)\right. \\ &\qquad \left. \pm \sin\left(\frac{\Delta\phi_r(-\omega_0)}{2}\right)\hat{b}_r(-\omega_0)\right)\end{aligned} \tag{9}$$

of the even and odd parts (superscripts ^{e,o} are associated to plus/minus sign) of $u_{0r}(\omega)$ and $i\vec{u}_r(\omega)$ at frequency ω_0.

Now, given the ISOP $\hat{j}$, we have to find the maximum of $Y(\omega_0)$ with respect to the two degrees of freedom given by $\hat{e}_c$. This mathematical issue is solved in the Appendix by maximizing $Y(\omega_0)^2$ (hence, $Y(\omega_0)$) through the method of Lagrange multipliers. The general solution for the compensator orientation is

$$\hat{e}_c = \frac{\left[\delta(\lambda_0 + b^2) + \gamma(\vec{a}\cdot\vec{b})\right]\vec{a} - \left[\gamma(\lambda_0 + a^2) + \delta(\vec{a}\cdot\vec{b})\right]\vec{b}}{D(\lambda_0)} \tag{10}$$

where $D(\lambda)$ is given in (22) and λ_0 is determined imposing unit magnitude for $\hat{e}_c$, as discussed in the Appendix. The corresponding Eye Opening is

$$Y = \left|\frac{\lambda_0}{D(\lambda_0)}\right|\left|\begin{bmatrix}\delta(\lambda_0 + b^2) + \gamma(\vec{a}\cdot\vec{b}) \\ \gamma(\lambda_0 + a^2) + \delta(\vec{a}\cdot\vec{b})\end{bmatrix}\right| \tag{11}$$

where $|\cdot|$ denotes the Euclidean norm. Special cases for the compensator orientation $\hat{e}_c$ and related EO Y are also discussed in the Appendix.

We note that the algorithm described above requires the knowledge of the Jones matrix $U_F(\omega_i)$ of the transmission fiber, evaluated at the frequencies $\omega_i \in \{-\omega_0, 0, +\omega_0\}$. These three measurements, along with the ISOP, provide all the parameters necessary for the maximization of (6), which, in general, yields the optimum condition (10) employed in all the simulations with OPMDC described in the following section.

B. Results

The principal benchmark to test the validity of the compensation algorithm described in the previous section is the evaluation of the outage probability versus the average DGD $\langle\Delta\tau\rangle$ of transmission fibers. We report in Fig. 2 the simulation results obtained for various values of the fixed compensator DGD $\Delta\tau_c$. OP is defined as the probability that the Sensitivity Penalty (SP), evaluated at $\mathrm{BER} = 10^{-10}$, exceeds 3 dB with respect to the back-to-back configuration. As to the transmission system, the preamplified receiver specifications are: optical and electrical filter bandwidths equal to $5/T_b$ and $0.65/T_b$, respectively, noise figure of 6 dB, and optical input SNR equal to 40 dB, resulting in a back-to-back sensitivity of -33.2 dBm. As to the OMPDC, its orientation is set so as to maximize (6), as described in the previous section, for every transmission fiber and ISOP configuration used to obtain SP values.

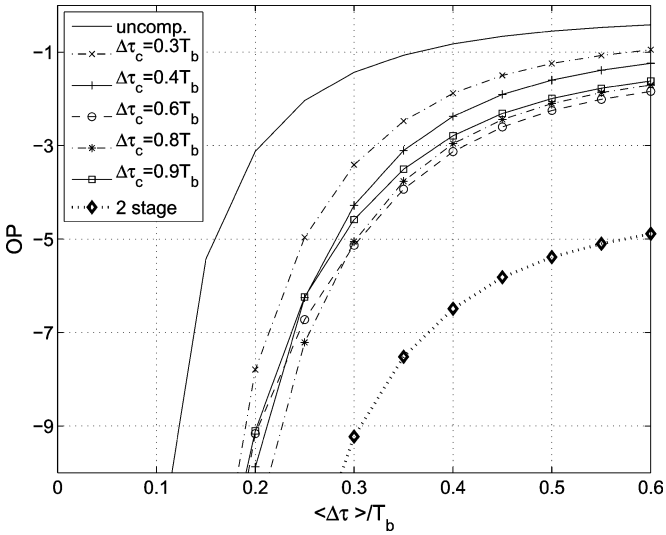

Fig. 2. Outage probability (OP) versus system average DGD: single-stage compensator with fixed DGD $\Delta\tau_c$ and double-stage compensator (described in Section III-A); uncompensated system performance is reported for comparison.

The OP curves in Fig. 2 were obtained through a semi-analytical technique described hereafter. In a first step, we ran the multivariate Multicanonical Monte Carlo (MMC) algorithm that we recently proposed in [7], which generates fiber samples, using the standard random waveplate model (RWM) with 100 plates, according to the known joint probability density function (pdf) $p(X,Y)$, where $(X,Y) = (|\vec{\Omega}|/\langle\Delta\tau\rangle, |\vec{\Omega}_\omega|/\langle\Delta\tau\rangle^2)$ are the normalized first- and second-order PMD vector magnitudes.[2] Such algorithm extends the enhanced MMC approach [19] to the multivariate case, driving the many free parameters of the RWM so as to produce rare fiber samples with an increased efficiency, with respect to the standard multivariate MMC algorithm [20], [21]. For a given average DGD $\langle\Delta\tau\rangle$, we let the algorithm explore the (X,Y) plane in an interval ($[0;7]\times[0;14]$) divided in 30×30 bins: emulated fibers covered 489 out of the 900 bins, as seen in Fig. 5 (lower left), and reproduced $p(X,Y)$ with good accuracy down to 10^{-25} [7]. During the process, in each of the finely spaced bins, we saved only the first RWM model encountered during the random walk in the MMC algo-

[2]A complete second-order description of PMD would require a third parameter θ_Ω, i.e., the angle between $\vec{\Omega}$ and $\vec{\Omega}_\omega$. We do not consider θ_Ω here, since, to our knowledge, an accurate expression for the joint pdf of the three parameters $(|\vec{\Omega}|, |\vec{\Omega}_\omega|, \theta_\Omega)$ is not known in the general case, while the bivariate pdf $p(|\vec{\Omega}|, |\vec{\Omega}_\omega|)$ can be efficiently evaluated as described in [18].

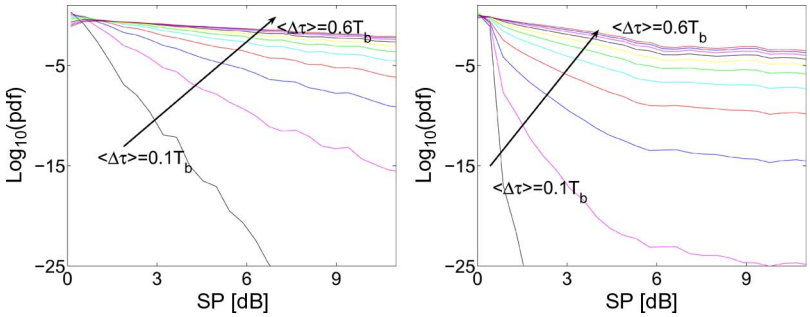

Fig. 3. Sensitivity penalty distributions for increasing average DGD of transmission fibers, for (left) an uncompensated and (right) compensated system ($\Delta\tau_c = 0.4T_b$).

rithm, and thus got a pool of 489 *representative* RWM fiber samples.[3] In the second step, we simulated NRZ transmission of a 32-bit PRBS on each fiber sample of the pool, repeating the simulation for 62 signal ISOPs uniformly tiling the Poincaré sphere. We thus obtained $489 \times 62 = 30318$ SP values from which we evaluated (in discrete form) the pdf

$$p(SP)dSP = \int\int\int\int I\left(SP\left(|\vec{\Omega}|, |\vec{\Omega}_\omega|, \theta_j, \epsilon_j\right)\right) p(\theta_j, \epsilon_j) \cdot p\left(\frac{|\vec{\Omega}|}{\langle\Delta\tau\rangle}, \frac{|\vec{\Omega}_\omega|}{\langle\Delta\tau\rangle^2}\right) d|\vec{\Omega}| d|\vec{\Omega}_\omega| d\theta_j d\epsilon_j \quad (12)$$

where $p(\theta_j, \epsilon_j)$ is the pdf of the ISOP azimuth and ellipticity, and $I(SP(|\vec{\Omega}|, |\vec{\Omega}_\omega|, \theta_j, \epsilon_j))$ is an indicator function, equal to 1 iff a model with given PMD values has produced a Penalty in the range dSP around the value SP for the given ISOP. The joint pdf of the first- and second-order PMD can be numerically evaluated as described in [18]. In the last step, we just vary $\langle\Delta\tau\rangle$, which warps the *weight* $p(X, Y)$ attributed to each fiber sample, and recalculate (12) accordingly, then integrate the SP distribution to get $P(OP) = P\{SP > 3\}$. As an example, we report in Fig. 3 the SP distribution for an uncompensated and compensated system with $\Delta\tau_c = 0.4T_b$, for various values of $\langle\Delta\tau\rangle$. The advantage of this technique is that the computational burden relies mainly on the first step; once the representative RWM fiber samples are available, the evaluation of each OP curve in Fig. 2 takes about 4 h on an old 800-MHz processor.

Assuming a target $\mathrm{OP} = 10^{-5}$ (corresponding to 5 min./year outage), the OP curve for an uncompensated system, reported for comparison in Fig. 2, shows that the maximum tolerable average DGD is around $0.15T_b$, a figure which is increased to about $0.3T_b$ by the use of a single-stage OPMDC with $\Delta\tau_c = 0.6T_b$. These figures are consistent with the *common wisdom* on optical PMD compensation. Similar figures are found in the vast technical literature (see, e.g., [5]), despite different approaches and different definitions of Outage.

A method employing MMC to estimate the OP of an OPMDC system, for fibers with a given $\langle\Delta\tau\rangle$, was first adopted by Lu *et al.* in [23]. The work of Secondini and Forestieri [24], though employing similar statistical techniques for generating fiber samples, aims at a direct estimation of OP, circumventing

[3]The value of θ_Ω is thus totally random, in each representative sample. We verified that its *a posteriori* distribution is symmetric around a peak value of 90°, indicating that the perpendicular component $\vec{\Omega}_{\omega\perp}$, related to PSP depolarization, is statistically dominant over the parallel component $\vec{\Omega}_{\omega||}$, related to PCD [22].

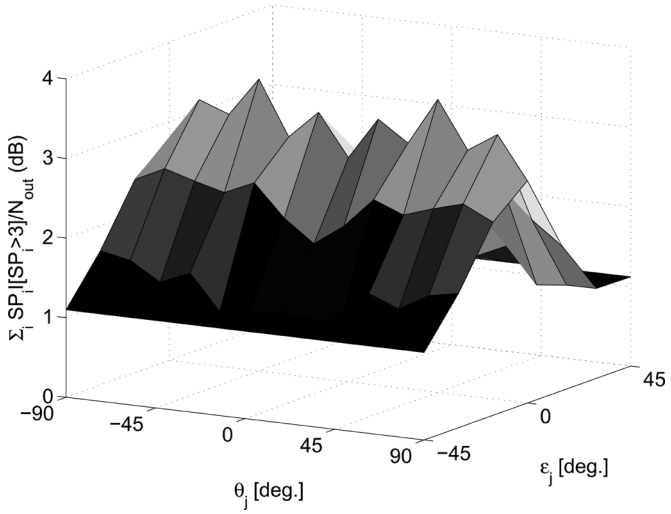

Fig. 4. Average sensitivity penalty (SP) versus ISOP: (unweighted) average evaluated over fiber samples causing outage ($\Delta\tau_c = 0.8T_b$), at least for one ISOP.

the need for a probabilistic description of PMD parameters. Despite this clear advantage, RWM fibers are dynamically generated in [24]; hence, it is not possible to perform an *a posteriori* analysis of simulation results to show how performance depends on the channel configuration, which is our next task. In fact, to understand the intrinsic limitations of single-stage OPMDC, it is important to investigate what are the joint configurations of transmission fiber and ISOP that yield large SP. While it is quite obvious that larger first- and second-order PMD values increase the penalty, it is not trivial to assess the vulnerability of different launch conditions (ISOP) in a system with higher order PMD. Fig. 4 reports the average SP of fibers versus ISOP, conditioned on outage. Precisely, for each ISOP, SP values obtained from simulations are averaged over those N_{out} fiber samples for which outage occured for at least one ISOP. Average is intended here as the occurrence ratio $\Sigma_i SP_i I(SP_i > 3)/N_{\mathrm{out}}$; fiber samples are not weighted with their probability $p(|\vec{\Omega}|, |\vec{\Omega}_\omega|)$, otherwise the contribution of samples with larger PMD and lower pdf would be masked in a statistical average. In Fig. 5 (lower left), the bins of the 489 simulated fiber samples are marked with dots, while the $N_{\mathrm{out}} = 124$ samples that cause outage, with $\Delta\tau_c = 0.8T_b$, are highlighted with circles. The SP versus ISOP plots for each sample, of which Fig. 4 is an average, are, in general, different. Among these, three meaningful cases are reported in Fig. 5:

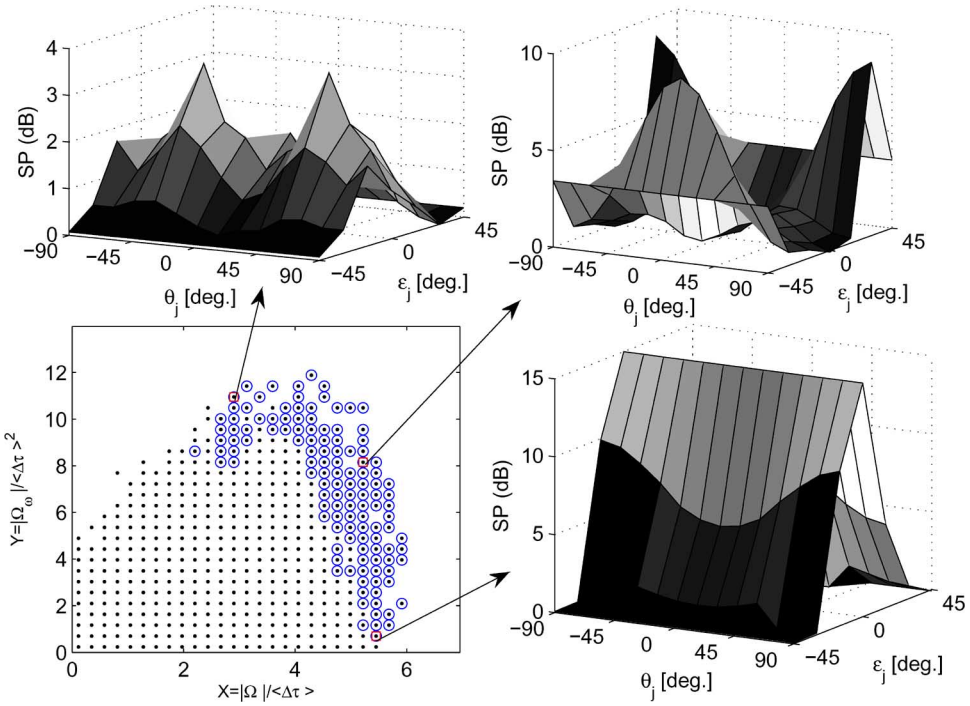

Fig. 5. (Lower left) Bins on the PMD plane (X, Y) including (dots) simulated fiber samples: circles highlight samples causing Outage after OPMDC with $\Delta\tau_c = 0.8T_b$. (Others) Plots of SP versus ISOP for outage cases with different amounts of first- and second-order PMD.

lower right is the typical case where first-order PMD dominates performance ($\hat{q}$ is a circular polarization in this case); upper right is a case where both first- and second-order PMD are large; upper left is a case where, given the line DGD, it is higher-order PMD that brings the ISOPs around $\vec{u}_r^e$ to outage. To get meaningful plots, the signal ISOP is measured relative to a frame of reference where $\hat{b}_r(\pm\omega_0)$ and $\hat{b}_r(0)$ lie on a plane parallel to the $(\hat{s}_1, \hat{s}_2)$ plane in Stokes space, and the vector $\vec{u}_r^e$ is aligned with $\hat{s}_2$. Fig. 4 shows that $\hat{j} \parallel \vec{u}_r^e$ is the most critical ISOP, on average. We discuss the peculiarities of such ISOP in the following section, with particular reference to the case of large second-order PMD, as in Fig. 5 (upper left).

C. Discussion

We wish now to interpret the peculiarity of the worst ISOP $\hat{j} \parallel \vec{u}_r^e$ in terms of the quantities defined in Section II-A, shedding some light on their physical meaning and pointing out what fiber samples are the most vulnerable.

Consider the case of a transmission fiber with only first-order PMD [i.e., similar to the case of Fig. 5 (lowe right)]: $\Delta\phi_r(\omega) = \Delta\tau\omega$ and $\hat{b}_r = \hat{q}_i$ is frequency independent. Hence, $u_{0r}^e = \cos(\Delta\tau\omega_0/2)$, $\vec{u}_r^o = \sin(\Delta\tau\omega_0/2)\hat{q}_i$, and $\vec{u}_r^e = \vec{0}$, $u_{0r}^o = 0$ result from (9). It is then obvious that $\hat{j} \perp \hat{q}_i$ [the circle $\varepsilon_j = 0$, in the frame of Fig. 5 (lower right), including $\hat{j} = \pm\hat{s}_2$] are the most critical ISOPs, corresponding to a 50% power splitting on the PSPs. To analyze the case of higher-order PMD, let us assume that $\Delta\phi_r(+\omega_0) = -\Delta\phi_r(-\omega_0)$.[4] Thus, (9) implies that $\vec{u}_r^{e,o} = \sin(\Delta\phi_r(\omega_0)/2)(\hat{b}_r(\omega_0) \mp \hat{b}_r(-\omega_0))/2$ are orthogonal vectors: $\vec{u}_r^o$ points in the *average eigenmode* direction, which plays the role played by the input PSP for first-order PMD, while $\vec{u}_r^e$ is related to the *eigenmodes depolarization*, and quantifies higher order PMD on the signal bandwidth.

Let us now evaluate the compensator behavior when the ISOP is aligned with the *eigenmodes depolarization*, i.e., $\hat{j} \parallel \vec{u}_r^e$ ($\hat{j} = \pm\hat{s}_2$, in Figs. 4 and 5): $(\vec{a} \cdot \vec{b}) = 0$ and $\gamma = 0$ result from (8), and the values of the Lagrange multiplier yielding a unit norm solution are $\lambda_{1,2} = -a^2 \mp \delta a$ and $\lambda_{3,4} = -b^2$. For the first two values, the standard solution (10) applies, which reduces to $\hat{e}_c = \mp\vec{a}/a$, yielding $Y = |\delta \pm a|$ in (11). Hence, two extreme values for the EO appear when $\hat{e}_c$ is co- or counter-aligned with the *average eigenmode* direction. Recalling the definitions of δ and $\vec{a}$, it is easily seen that the best EO is

$$Y = |\delta + a| \le \left|\cos\left(\frac{\Delta\phi_r(\omega_0) - \Delta\tau_c\omega_0}{2}\right)\right| = Y_{\mathrm{PMF}} \quad (13)$$

with equality holding if and only if the eigenmode values $\hat{b}_r(\pm\omega_0)$ coincide. This latter case corresponds to a null *eigenmodes depolarization*, where compensation reduces to contrasting a *quasi-first-order* PMD fiber by a counter-aligned PMF. For the other two solutions $\lambda_{3,4} = -b^2$, $D(\lambda_{3,4}) = 0$, (25) holds and we are in the special case discussed in the Appendix. Hence, solution (26) applies and, after calculating k, the EO (27) is $Y = \sqrt{\delta^2 + b^2 + \delta^2 a^2/(b^2 - a^2)}$. This becomes the best solution when the *eigenmodes depolarization* increases, since a decreases and so does (13). In the unlucky case that $\hat{b}_r(+\omega_0) = -\hat{b}_r(-\omega_0)$ are opposite on the Poincaré sphere (a case that we will refer to as *maximum depolarization*) $\vec{a} = \vec{0}$ and the best EO reduces to

$$Y = \sqrt{\delta^2 + b^2} = \left|\cos\left(\frac{\Delta\phi_r(\omega_0)}{2}\right)\right| = Y_{\mathrm{unc}} \quad (14)$$

[4]Note that the retardation $\Delta\phi_r(\omega) = \Delta\tau\omega + \Delta\tau'\omega^2/2 + \Delta\phi_r'''(0)\omega^3/3! + \ldots$ is well approximated, on the signal bandwidth, by a few terms of the Taylor series expansion, at least for DGDs being a fraction of the bit-time. If a third-order expansion holds for $\Delta\phi_r(\omega)$ and the PCD $\Delta\tau'$ is negligible, then $\Delta\phi_r(\omega)$ is an odd function.

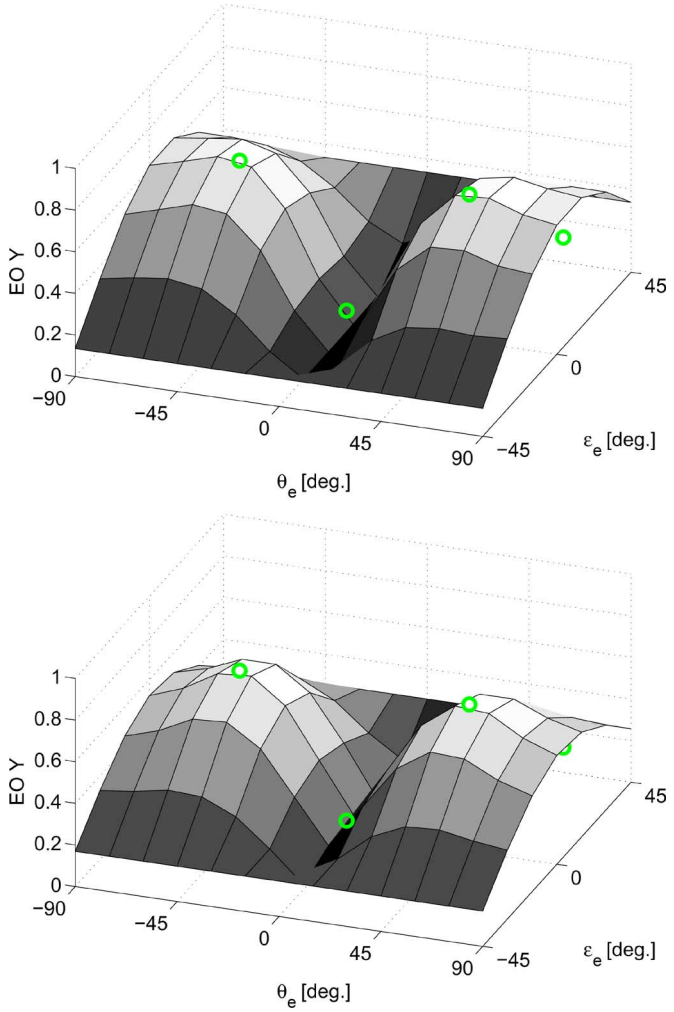

Fig. 6. EO as a function of compensator orientation, for a fiber sample with $\hat{j} \parallel \vec{u}_r^e$ ($\hat{s}_2$, in figure): (top) simulation results; (bottom) analytical plot of the GCF (6). Circles identify $\hat{e}_c$ positions associated to extreme EO values and are computed with the described algorithm.

which is the value obtained for an uncompensated transmission fiber, meaning that compensation is totally ineffective for this channel-ISOP configuration. In fact, the special solution (26) reduces to $\hat{e}_c = \pm\hat{b} = \pm\hat{j}$ in this case, i.e., the compensator gets aligned to the ISOP so as to produce "minimum damage."

The case of *maximum depolarization* deserves a special discussion. It is characterized by $\vec{u}_r^o = \vec{0}$, which greatly simplifies the analysis since it implies $\gamma = 0$, $\vec{a} = \vec{0}$, making $Y = \sqrt{\delta^2 + (\vec{b} \cdot \hat{e}_c)^2}$ in (6), from which $\hat{e}_c = \pm\hat{b}$ are clearly the best compensator orientations. The associated maximum EO $Y_{\max} = \sqrt{\delta^2 + b^2}$ basically depends on the angle between $\hat{j}$ and the *eigenmodes depolarization* $\vec{u}_r^e$, which determines the magnitude of $\vec{b}$ in (8). The best ISOPs are $\hat{j} \perp \vec{u}_r^e$, while the two worst ISOPs $\hat{j} \parallel \vec{u}_r^e$ ($\pm\hat{s}_2$, in the frame of Figs. 4 and 5) yield $Y_{\max} = Y_{\text{unc}}$ as in (14), making compensation totally ineffective.

A demonstration of these assertions can be seen in Fig. 6, where the EO Y is obtained by simulation (top) and analytically from the GCF (bottom), on a specific fiber sample, versus the compensator azimuth and ellipticity (θ_e, ϵ_e), using the same frame of reference as in Fig. 4, and a compensator DGD $\Delta\tau_c = 0.8T_b$. The fiber sample under test is the same as Fig. 5 (upper left), characterized by strong second-order PMD ($|\vec{\Omega}| = 0.53T_b$, $|\vec{\Omega}_\omega| = 0.37T_b^2$) and eigenmodes depolarization ($|\vec{u}_r^e|$ is twice as large as $|\vec{u}_r^o|$). Although depolarization is not maximum in this example ($\hat{b}(\pm\omega_0)$ form an angle of 125°), the analytical results derived above can still be applied. In fact, in the simulation we chose the worst ISOP $\hat{j} \parallel \vec{u}_r^e$, which gives $SP = 3.55$ dB in Fig. 5, corresponding to the best EO $Y_{\max} = 0.71$ in Fig. 6 (top), obtained from the compensator position $\hat{e}_c = -\hat{j}$ ($-\hat{s}_2$ in the chosen frame of reference). The value $Y_{\max}$ is slightly larger than the analytical result $Y_{\text{unc}} = 0.69$ predicted by the GCF approximation (14). Since in real cases the signal is not a sinusoid at ω_0 as assumed in (6), some benefit can in general be expected from compensation. However, in this particular example, we checked by simulation that a slightly better EO value $Y = 0.72$ is obtained by removing the compensator. The four circles in Fig. 6 identify the analytical solutions calculated off-line and show the ability of the described algorithm to spot out the global maxima as well as a local minimum and a saddle point at $\hat{e}_c = \pm\hat{a}$.

The analytical plot of (6) versus $\hat{e}_c$, reported in Fig. 6 (bottom) faithfully reproduces the shape of Fig. 6 (top). The maximum absolute deviation 0.14 happens at the global minimum, where the eye closure penalty is very large and the GCF looses accuracy. However, as noted in Section II-A, the effectiveness of the approach described in Section II-A relies on the accuracy of the GCF (6) in reproducing *the shape* of the EO surface obtained by simulation, especially around its maxima. In all the fiber-ISOP configurations that we tested, despite discrepancies found around the EO minima, the accuracy of the best estimated EO is within 0.15 and the optimal compensator position is always correctly found.

III. Double-Stage Compensator

A. Theory

Using a single-stage OPMDC with a given $\Delta\tau_c$, system outage is systematically produced whenever a fiber sample with sufficiently large DGD is at hand, as in the two subplots on the right side of Fig. 5. On the other hand, when the line DGD is sufficiently small that it could be effectively contrasted by the OPMDC, as in the case of Fig. 5 (upper left), we have seen in Section II-C how the most critical situation to compensate is the one described by odd retardation $\Delta\phi_r$ and *maximum depolarization*, plus a signal ISOP $\hat{j}$ aligned with either $\hat{b}_r(\pm\omega_0)$. Similar channel configurations cannot be effectively equalized by a single-stage OPMDC and their probability of occurrence contributes significantly to the system outage probability.

One possible strategy for designing a double-stage OPMDC that is able to contrast these channel configurations is the one we proposed in [25]. Its goal is to make the overall *extracted* matrix of the transmission line plus compensator $U_t(\pm\omega_0) = U_t(0) = \sigma_0$ equal to the identity matrix, at the two edge frequencies $\pm\omega_0$. If such a condition is met, then $Y(\omega_0) = 1$ in (6) is thus maximized and $U_t(\omega)$ should be close to the identity on the whole bandwidth $[-\omega_0; \omega_0]$: how *close* depends on the fiber average PMD. The idea behind this double-stage OPMDC, whose schematic diagram is reported in Fig. 1(b), is that the two

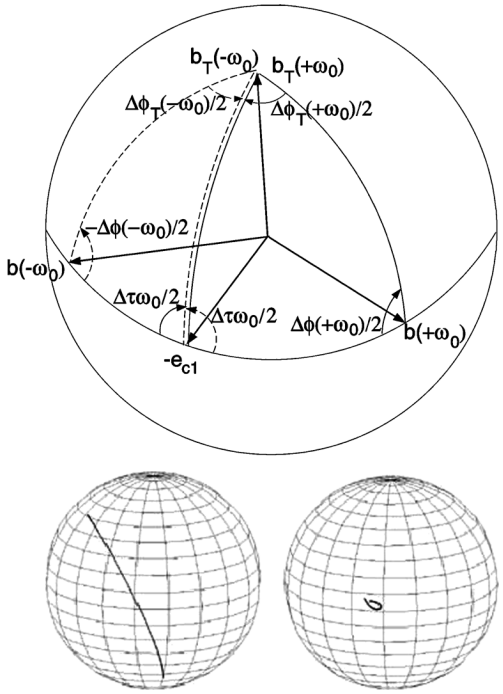

Fig. 7. (Top) Geometrical triangles showing the principle of operation of the first compensator-stage: depolarized $\hat{b}(\pm(\omega_0)$ are brought on a single point after first stage. (Bottom) Simulation results: eigenmode trace for a RWM fiber sample with strong depolarization, before and after application of the first stage.

stages perform conceptually different actions. The task of the first stage, with DGD $\Delta\tau_{c1}$ and PSP $\hat{e}_{c1}$ is to *bring together* the fiber eigenmodes $\hat{b}_r(\pm\omega_0)$ on a single point $\hat{b}_T$ of the Poincaré sphere, hence reducing the fiber plus first-stage to a *quasi-first-order* PMD system; the PSP $\hat{e}_{c2}$ of the second stage will be then counter aligned to $\hat{b}_T$ and its DGD $\Delta\tau_{c2}$ will constrast the overall residual retardation $\Delta\phi_T$. Choosing a variable $\Delta\tau_{c2}$ implies five degrees of freedom for the compensator, three being the angles of the PC placed between transmission fiber and OPMDC and the fifth being an optical rotator placed between the two OPMDC stages, which determines the angle between $\hat{e}_{c1}$ and $\hat{e}_{c2}$.

The task performed by the first stage can be visualized on the Poincaré sphere of Fig. 7 (top). Assume that $\underline{u}_c$ in (5) represents the Pauli vector of the first stage, and recall that the concatenation rule (5) has a simple geometrical interpretation in terms of spherical trigonometry. Based on well known geometrical theorems [12], [26], it can be shown [9] that the eigenmode and half-retardation of the product matrix $U_{c1}(\omega_0)U_r(\omega_0) = \exp\{-(i/2)\Delta\phi_T(\omega_0)(\hat{b}_T(\omega_0)\cdot\vec{\sigma})\}$ coincide with the third vertex and angle of the spherical triangle plotted with solid-line in Fig. 7 (top), whose other two vertices and angles are the eigenmode and half-retardation of the multiplied matrices, with the sign conventions of ([9, Fig.15]). Note that since the edges of a spherical triangle are portions of *great circles*, by rotating the sphere of Fig. 7 (top), there are eight possible triangles on which such geometrical relations can be equivalently visualized. Now, assume, as done in Section II-C, that $\Delta\phi_r(+\omega_0) = -\Delta\phi_r(-\omega_0)$. Then if we place $\hat{e}_{c1}$ midway between $\hat{b}_r(-\omega_0)$ and $\hat{b}_r(+\omega_0)$, one geometrical construction for finding $\Delta\phi_T(-\omega_0)/2$ and $\hat{b}_T(-\omega_0)$ from the concatenation rule (5) at frequency $-\omega_0$ is the mirror image of the one just described for $+\omega_0$, and thus coincides with the dashed-line spherical triangle of Fig. 7 (top). The choice we made for $\hat{e}_{c1}$ implies that $(\hat{b}_r(-\omega_0), \hat{e}_{c1}, \hat{b}_r(+\omega_0))$ lie on the same *great circle*, hence the angles $\Delta\tau_{c1}\omega_0/2$ must be 90 degrees, so that $\hat{b}_T(\pm\omega_0)$ coincide. The resulting settings for the first stage are

$$\begin{aligned}\Delta\tau_{c1} &= T_b\\ \hat{e}_{c1} &\| -\left(\hat{b}_r(+\omega_0)+\hat{b}_r(-\omega_0)\right).\end{aligned} \tag{15}$$

Looking at Fig. 7 (top), it is understood that, as long as $\hat{b}_r(+\omega_0) \neq -\hat{b}_r(-\omega_0)$, a different choice from that of (15) would be possible for the first stage, e.g., by decreasing (increasing) $\Delta\tau_{c1}$ and consequently moving $\hat{e}_{c1}$ downwards (upwards) along the great circle linking $\hat{e}_{c1}$ and $\hat{b}_T(\pm\omega_0)$. Anyway, it can be easily seen that the choice (15) of building *right spherical triangles*, is the only one ensuring that the geometrical construction in Fig. 7 (top) still holds when the transmission fiber eigenmodes approach *maximum depolarization*, i.e., when $\hat{b}_r(+\omega_0) \simeq -\hat{b}_r(-\omega_0)$. This is, indeed, the most critical situation discussed in the previous section, for which we want the first compensator stage to be effective, hence the choice of having its DGD equal to one bit-time is mandatory.

The DGD and eigenmode of the second stage are matched to the overall retardation $\Delta\phi_T(\omega_0)$ and eigenmode $\hat{b}_T(\omega_0)$ of transmission fiber plus first-stage. Their analytical expressions are obtained by plugging (15) into the chain rule (5)

$$\begin{aligned}\Delta\tau_{c2} &= \frac{\Delta\phi_T(\omega_0)}{\omega_0}\\ &= \frac{2}{\omega_0}\arccos\left(\sin\left(\frac{\Delta\phi_r(\omega_0)}{2}\right)\hat{b}_r(\omega_0)\cdot\hat{e}_{c1}\right)\\ \hat{e}_{c2} &= -\hat{b}_T(\omega_0) = \frac{-1}{\sin(\Delta\tau_{c2}\omega_0/2)}\\ &\quad\cdot\left[\cos\left(\frac{\Delta\phi_r(\omega_0)}{2}\right)\hat{e}_{c1}\right.\\ &\quad\left.-\sin\left(\frac{\Delta\phi_r(\omega_0)}{2}\right)\hat{b}_r(\omega_0)\times\hat{e}_{c1}\right]\end{aligned} \tag{16}$$

from which the Jones matrix of the second stage $U_{c2}(\omega_0) = \exp\{-(i/2)\Delta\tau_{c2}\omega_0(\hat{e}_{c2}\cdot\vec{\sigma})\}$ equals the inverse $(U_{c1}(\omega_0)U_r(\omega_0))^\dagger = \exp\{+(i/2)\Delta\phi_T(\omega_0)(\hat{b}_T(\omega_0)\cdot\vec{\sigma})\}$, and similarly for $-\omega_0$, thus equalizing the transmission fiber plus first stage at $\pm\omega_0$, as prescribed.

The control algorithm (15), (16) for the double-stage OPMDC relies on the same quantities employed to control the single-stage OPMDC: $\Delta\phi_r(\pm\omega_0)$ and $\hat{b}_r(\pm\omega_0)$. If $\Delta\phi_r(\pm\omega_0)$ are opposite, as assumed above, then, using the quantities defined in (9), one can set $\hat{e}_{c1} = -\hat{u}_r^o$ in (15) while $u_{0r}^e \pm u_{0r}^o$ and $\vec{u}_r^e \pm \vec{u}_r^o$ can be substituted to $\cos(\Delta\phi_r(\omega_0)/2)$ and $\sin(\Delta\phi_r(\omega_0)/2)\hat{b}_r(\omega_0)$ in (16), with either $\pm$ sign yielding the same result. Although the condition assumed for $\Delta\phi_r(\pm\omega_0)$ is not strictly met by actual transmission fibers, the principle of operation for the first OPMDC stage is still valid: Fig. 7 (bottom) shows the eigenmode trace, on the bandwidth $[-\omega_0;\omega_0]$, for an emulated RWM fiber sample. The strong depolarization of $\hat{b}_r(\omega)$ (left) is reduced to an almost frequency-independent (i.e., *quasi-first-order* PMD) $\hat{b}_T(\omega)$ (right) by the first compensator stage, although the resulting $\hat{b}_T(\pm\omega_0)$ do not coincide due to mismatched values of $\Delta\phi_r(\pm\omega_0)$.

B. Results and Discussion

The procedure for evaluating the Outage Probability with the double-stage OPMDC described in Section III-A was the same as that described in Section II-B. We used (15) and (16) to drive the compensator stages. Note that, for the double-stage OPMDC, the compensator control algorithm is not dependent on the ISOP anymore. The resulting OP was the bottommost curve plotted in Fig. 2 versus the average DGD of transmission fibers. Results show that for an OP $= 10^{-5}$, the tolerance of the double-stage compensator is of the order of half bit-time, significantly extending the reach of the single-stage compensator described in Section II. The presence of a second stage with variable DGD makes the compensator robust to channel configurations with small $|\Omega_\omega|$ and large DGD $|\Omega|$. In such situations of *quasi-first-order* PMD, an almost constant $\hat{b}_r$ in (15) yields $\hat{e}_{c1}$ counter-aligned with it, hence the line DGD is subtracted from the DGD $\Delta\tau_{c1} = T_b$ of the first stage. At the same time, the first equation in (16) ensures that $\Delta\tau_{c2} = T - \Delta\phi_r(\omega_0)/\omega_0$, where $\Delta\phi_r(\omega_0)/\omega_0$ should be regarded as the *effective DGD* of the transmission fiber at frequency ω_0. Finally, the second equation in (16) makes the PSP of the second stage $\hat{e}_{c2} = -\hat{e}_{c1}$ counter-aligned to the first, so that the DGDs $\Delta\phi_r(\omega_0)/\omega_0$, $-\Delta\tau_{c1}$ and $\Delta\tau_{c2}$ algebraically add together to produce a null retardation at $\pm\omega_0$. Experimental results, in fact, confirm that the rare cases in which the Sensitivity Penalty exceeds 3 dB are associated with fiber samples with very large second-order PMD, where a large $|\vec{q}'| = 2|\vec{b}_r'(0)|$ implies relevant eigenmodes depolarization. One reason for the partial failure of the double-stage OPMDC in these cases can be a large value of the PCD $\Delta\tau' = \Delta\phi_r''(0)$[5] which makes the retardation $\Delta\phi_r(-\omega_0)$ significantly different from $-\Delta\phi_r(+\omega_0)$, in contrast with the hypothesis assumed in deriving the control algorithm (15), (16).

The presence in the first stage of a PMF section with a DGD as large as the bit time, as prescribed by (15), may seem at first surprising. It is worth noting that other works in the literature have reached similar conclusions, despite a completely different approach to compensation. For instance, [27] presents an adaptive control criterion for a multistage OPMDC which aims at minimizing the mean square error of detected symbols after the optical receiver. The exemplification on a three-stage OPMDC in [27] shows that the first stage may have a large DGD, in the order of the bit duration, and the other two stages have a DGD in the order of half the bit time.

Regarding the approach that we followed, it is clear that an effective compensation is achieved whenever the frequency-dependent part of the Jones matrix of the transmission fiber is equalized by the Jones matrix of the compensator on the whole signal bandwidth. For ease of analysis, and consistently with the maximization of the EO (6) pursued in Section II-A, we concentrated on the frequencies $\pm\omega_0$, plus $\omega = 0$, hence realizing a *discrete frequency-domain equalization strategy*. A *continuous frequency-domain equalization strategy* is, for instance, the one adopted in [28], since it aims at maximizing the overall integrated (and weighted) electrical power spectrum, so as to equalize the *spectral hole* due to first-order PMD in the received signal, or other linear distortions caused by higher-order PMD; the approach in [28], however, permits little insight into the compensator operation. Whether the objective of an OPMDC is to equalize the channel at some discrete points, as we do, or on a continuous frequency interval of the transmitted signal spectrum, it is, however, important to remark that the compensator *budget*, i.e., quantified by the DGD of its stages, should not be spent on equalizing only at the carrier frequency $\omega = 0$ and its neighborhood, as would happen in a control criterion based on the PMD vector and its derivatives.

Regarding our approach of separating the tasks of the OPMDC stages, we would also like to cite the work of Shtaif *et al.* [29], which presents a three-stage OPMDC where the second stage compensates first-order PMD while the first and third stages compensate higher-order PMD. In fact, such OMPDC compensates high-order PMD by ideally inverting the Jones matrix of the transmission fiber, assuming that it can be modeled with a linear retardation $\Delta\phi_r(\omega) = \Delta\tau_r\omega$ and eigenmode $\hat{b}_r(\omega)$ rotating at constant speed in a circle (not necessarily a *great-circle*). Such a model has been called *rotation model* in [9]. Reduced complexity, with only 5 degrees of freedom for the three stages, is achieved in [29] by exploiting the symmetries of the compensator Jones matrix.

IV. Conclusion

We analyzed single- and double-stage optical PMD compensators, whose performance is already assessed in the literature, from a novel point of view, relying on a representation of the transmission fiber in terms of *extracted eigenmodes and retardation*. As opposed to the classical description in terms of the PMD vector and its derivatives (to which we anyhow relate the analytical results, when possible), this approach aims at equalizing the transmission fiber Jones matrix on a large signal bandwidth. At the same time, the adopted perspective permits a great deal of analytical insight.

First, we derived a control algorithm for a single-stage optical PMD compensator with fixed DGD, based on the maximization of the Eye Opening, as provided by the *generalized Chen formula*. The analytic solutions thus found correctly reproduce simulation results and the control algorithm drives the compensator to yield the expected Outage Probability. We justify analytically the experimental evidence that for certain critical transmission fibers (i.e., those with *maximum depolarization*) and States of Polarization of the input signal (i.e., those aligned with the *eigenmodes depolarization*), a single-stage compensator is totally ineffective and produces the same Eye Opening as in an uncompensated system.

To overcome these limitations, we analyzed a double-stage compensator with five degrees of freedom. Consistently with the target of the single-stage, the compensation strategy aims at equalizing the system matrix at three discrete frequencies, at the center and edges of the signal bandwidth. The control algorithm is based on a simple interpretation in terms of spherical geometry. We showed how the tasks of the two stages are conceptually distinct: the first stage aims at eliminating *eigenmodes depolarization* while the second compensates the residual PMD, which is *quasi-first-order*. Somehow surprisingly, we showed that the fixed DGD of the first stage must be as large as the bit

[5]Note that the PCD is still related to second-order PMD, since $|\Omega_\omega| = |\Delta\tau\vec{q}' + \Delta\tau'\hat{q}| = \sqrt{\Delta\tau^2|\vec{q}'|^2 + (\Delta\tau')^2}$ (the unit-magnitude PSP $\hat{q}$ is orthogonal to its derivative $\vec{q}'$).

period. For the same target outage, the double-stage compensator enhances the system margin of tolerable average PMD as expected.

In both cases, the outage probability was quantified through a fast semi-analytical technique, based on a pool of representative fiber samples obtained using a novel multivariate Multicanonical Monte Carlo technique.

Appendix
Optimization of the Eye Opening for the Single-Stage Compensator

The problem here is to maximize a non-negative scalar function $Y(\vec{x})$, or equivalently maximize $Y^2(\vec{x})$, with respect to the unknown $\vec{x} = \hat{e}_c$, subject to the constraint $|\vec{x}| = 1$. The mathematical tool for such constrained maximization is the method of Lagrange multipliers. We build the function

$$f(\vec{x}) = Y^2(\vec{x}) + \lambda(\vec{x}^T\vec{x} - 1) \tag{17}$$

and look for its unconstrained extrema by solving the gradient equation

$$\vec{\nabla} f \triangleq \begin{bmatrix} \partial f/\partial x_1 \\ \partial f/\partial x_2 \\ \partial f/\partial x_3 \end{bmatrix} = \vec{0}. \tag{18}$$

Once a solution $\vec{x}_s(\lambda)$ is obtained, the Lagrange multiplier λ is found by imposing that such solution satisfies the constraint $|\vec{x}_s(\lambda)|^2 = 1$. Recalling (6) and (7), the solution of (18) is

$$\vec{x}_s(\lambda) = \frac{1}{\lambda}c\vec{a} - \frac{1}{\lambda}(\vec{o}\cdot\hat{j})\vec{b} \tag{19}$$

where the argument ω_0 is omitted for brevity. Plugging (19) into (7) in place of $\hat{e}_c$, we get the following system of two equations:

$$\begin{bmatrix} (\lambda + a^2) & -(\vec{a}\cdot\vec{b}) \\ -(\vec{a}\cdot\vec{b}) & (\lambda + b^2) \end{bmatrix} \begin{bmatrix} c \\ (\vec{o}\cdot\hat{j}) \end{bmatrix} = \lambda \begin{bmatrix} \delta \\ \gamma \end{bmatrix} \tag{20}$$

a and b being the magnitude of vectors $\vec{a}$ and $\vec{b}$, both ≤ 1, whose solution is

$$\begin{bmatrix} c \\ (\vec{o}\cdot\hat{j}) \end{bmatrix} = \frac{\lambda}{D(\lambda)} \begin{bmatrix} \delta(\lambda + b^2) + \gamma(\vec{a}\cdot\vec{b}) \\ \gamma(\lambda + a^2) + \delta(\vec{a}\cdot\vec{b}) \end{bmatrix} \tag{21}$$

where

$$D(\lambda) = (\lambda + a^2)(\lambda + b^2) - (\vec{a}\cdot\vec{b})^2 \tag{22}$$

is the determinant of the real and symmetric system matrix in (20). Substituting (21) in (19) yields the unconstrained solution

$$\vec{x}_s(\lambda) = \frac{\left[\delta(\lambda + b^2) + \gamma(\vec{a}\cdot\vec{b})\right]\vec{a} - \left[\gamma(\lambda + a^2) + \delta(\vec{a}\cdot\vec{b})\right]\vec{b}}{D(\lambda)} \tag{23}$$

clearly showing that the optimal compensator position always lies in the plane spanned by $(\vec{a}, \vec{b})$[6]

$$(\lambda I + \vec{a}\vec{a}^T + \vec{b}\vec{b}^T)\vec{x} = (\delta\vec{a} - \gamma\vec{b}). \tag{24}$$

The Lagrange multiplier is determined by imposing that $\vec{x}_s$ has unit norm, hence by equating $D^2(\lambda) = P(\lambda)$, where $P(\lambda)$ is the squared magnitude of the numerator in (23). Both $D(\lambda)$ and $P(\lambda)$ are second-order polynomials in λ, with positive coefficients. Geometrically, they define upward concave parabolae with vertices $(\lambda_D < 0, D(\lambda_D) \leq 0)$ and $(\lambda_P < 0, P(\lambda_P) \geq 0)$, respectively. There can be up to four intersection points, whose abscissae $\lambda_{1,2,3,4}$ (of which at least two are negative), are the solutions of the fourth-order equation $D^2(\lambda) = P(\lambda)$. These correspond to stationary points for the function $Y^2(\vec{x}_s(\lambda))$, which can be either maxima, minima or saddle points. The corresponding values for the eye opening (6) are simply the Euclidean norm of the vector in (21). The compensator control algorithm tests the four roots and selects the λ_0 yielding the largest EO $Y(\lambda_0)$, as reported in (11).[7] Hence, in standard cases, $\hat{e}_c = \vec{x}_s(\lambda_0)$ in (10) is the sought compensator orientation.

The only case in which the standard solution (10) does not hold is when the determinant $D(\lambda_0)$ is null. Since it must be $P(\lambda_0) = 0$ at the same time (geometrically, the vertex of P intersects D^2 at two coinciding points on the λ axis), the vector in the numerator of (23) is null. If $\vec{a}$ is not parallel to $\vec{b}$, then it must be

$$\left[\delta(\lambda_0 + b^2) + \gamma(\vec{a}\cdot\vec{b})\right] = \left[\gamma(\lambda_0 + a^2) + \delta(\vec{a}\cdot\vec{b})\right] = 0 \tag{25}$$

from which the sought λ_0 is found. A necessary and sufficient condition for (25) is $\delta\gamma(a^2 - b^2) = (\gamma^2 - \delta^2)(\vec{a}\cdot\vec{b})$, which we use in our software to discriminate the special cases before calculating λ_0. Equation (25) implies that the system (20) is undetermined. Nonetheless, the solution in the limit $\vec{x}_l(\lambda_0) = \lim_{\lambda\to\lambda_0}\vec{x}_s(\lambda) = (\delta\vec{a} - \gamma\vec{b})/(2\lambda_0 + a^2 + b^2)$, obtained by applying de L'Hospital's rule to the general solution (23), is seen to satisfy (24), hence to solve (18). Such solution has not unit norm, but, under condition $D(\lambda) = 0$, the system matrix in (24) also has null determinant and its null-space is proportional to the vector $\vec{c} = (\gamma\vec{a} + \delta\vec{b})$. Hence, iff $|\vec{x}_l(\lambda_0)| \leq 1$, a term $k\vec{c}$ can be added to $\vec{x}_l(\lambda_0)$, with k so as to make

$$\hat{e}_c = \left(\frac{\delta\vec{a} - \gamma\vec{b}}{2\lambda_0 + a^2 + b^2}\right) + k(\gamma\vec{a} + \delta\vec{b}) \tag{26}$$

a unit-magnitude solution of (24). Note that the two terms in (26) are orthogonal, since (25) implies that their inner product is null. Hence, solutions (26) always occur in pairs, with opposite $\pm k$ values. Substituting (26) in (7) and then in (6), the corresponding Eye Opening is

$$Y = \sqrt{(\delta^2 + \gamma^2)\left(\frac{|\lambda_0|^2}{(2\lambda_0 + a^2 + b^2)^2} + k^2|\lambda_0|^2\right)} \tag{27}$$

that for $k = 0$ coincides with the $\lim_{\lambda\to\lambda_0}$ of the standard Y expression in (11). In the subcase where $D(\lambda_0) = P(\lambda_0) = 0$ and $\vec{a} \parallel \vec{b}$ (including cases where one of the two vectors is null), ((26), (27)) still hold, but are further simplified since it can be shown that $\delta\vec{a} - \gamma\vec{b} = \vec{0}$, hence $\hat{e}_c$ reduces to the second (null-space) term only in (26) while the fraction term in (27) reduces to 1, since $\lambda_0 = -a^2 - b^2$ is the only nonzero solution.

Note that the EO can be always expressed as $Y = |\lambda_0|\sqrt{x_a^2 + x_b^2}$, where $x_{a,b}$ are the coordinates of $\hat{e}_c =$

[6]As an alternative procedure, we could have plugged c and $(\vec{o}\cdot\hat{j})$ from (7) into (19), with the unknown $\vec{x}$ in place of $\hat{e}_c$, to get (24), that can be solved by inverting the 3×3 matrix (see, e.g., [30, p. 130]), obtaining the same solution (23).

[7]In all the cases we tried, we always found that the most negative solution $\lambda_0 = \lambda_1$ is the one associated with the optimal compensator behavior. We have not found a mathematical explanation for this, although the solution λ_1 with largest modulus clearly maximizes the term $|\lambda|$ in Y.

$x_a\vec{a}+x_b\vec{b}$ with respect to the (nonorthogonal, in general) frame of reference $(\vec{a},\vec{b})$; such expression embraces both (11) with the standard solution (10), and (27) in the special case (26).

ACKNOWLEDGMENT

The authors would like to thank E. Corbel, S. Lanne, and S. Bigo, from Alcatel-Lucent Research and Innovation in Villarceaux, Nozay (France), for helpful discussions and comments.

REFERENCES

[1] X. Liu, C. Xie, and A. J. van Wijngaarden, "Multichannel PMD mitigation and outage reduction through FEC with sub-burst-error-correction period PMD scrambling," *IEEE Photon. Technol. Lett.*, vol. 16, no. 9, pp. 2183–2185, Sep. 2004.

[2] A. Galtarossa, L. Palmieri, and A. Pizzinat, "Optimized spinning design for low PMD fibers: An analytical approach," *J. Lightw. Technol.*, vol. 19, no. 10, pp. 1502–1512, Oct. 2001.

[3] M. Jager, T. Rankl, J. Speidel, H. Bulow, and F. Buchali, "Performance of Turbo Equalizers for Optical PMD Channels," *J. Lightw. Technol.*, vol. 24, no. 3, pp. 1226–1236, Mar. 2006.

[4] R. Noé, D. Sandel, M. Yoshida-Dierolf, S. Hinz, V. Mirvoda, A. Schöpflin, C. Glingener, E. Gottwald, C. Scheerer, G. Fischer, T. Weyrauch, and W. Haase, "Polarization mode dispersion compensation at 10, 20, and 40 Gb/s with various optical equalizers," *J. Lightw. Technol.*, vol. 17, no. 9, pp. 1602–1615, Sep. 1999.

[5] H. Sunnerud, C. Xie, M. Karlsson, R. Samuelsson, and P. A. Andrekson, "A comparison between different PMD compensation techniques," *IEEE J. Lightw. Technol.*, vol. 20, no. 3, pp. 368–378, Mar. 2002.

[6] C. K. Madsen, P. Oswald, S. Chandrasekhar, L. Buhl, M. Cappuzzo, E. J. Laskowski, E. Chen, L. Gomez, A. Griffin, A. Kasper, L. Stulz, and A. Wong-Foy, "Real-time PMD measurement using an integrated wavelength-scanning polarimeter," in *Proc. ECOC*, Sep. 2003, vol. 4, pp. 958–959.

[7] A. Vannucci, N. Rossi, and A. Bononi, "Emulazione e statistiche della PMD attraverso algoritmi multicanonici multivariati," in *Proc. Fotonica* (in Italian), May 2007, pp. 517–520.

[8] J. P. Gordon and H. Kogelnik, "PMD fundamentals: Polarization mode dispersion in optical fibers," *Proc. Nat. Acad. Sci.*, vol. 97, pp. 4541–4550, Apr. 2000.

[9] A. Bononi and A. Vannucci, "Is there life beyond the principal states of polarization?," *Opt. Fiber Technol.*, vol. 8, pp. 257–294, Oct. 2002.

[10] H. Kogelnik, L. E. Nelson, and J. P. Gordon, "Emulation and inversion of polarization-mode dispersion," *J. Lightw. Technol.*, vol. 21, no. 2, pp. 482–495, Feb. 2003.

[11] A. Vannucci and A. Bononi, "Statistical characterization of the Jones matrix of long fibers affected by polarization mode dispersion (PMD)," *J. Lightw. Technol.*, vol. 20, no. 5, pp. 811–821, May 2002.

[12] J. B. Kuipers, *Quaternions and Rotation Sequences*. Princeton, NJ: Princeton Univ. Press, 1999.

[13] M. Karlsson and M. Petersson, "Quaternion approach to PMD and PDL phenomena in optical fiber systems," *J. Lightw. Technol.*, vol. 22, no. 4, pp. 1137–1146, Apr. 2004.

[14] A. Eyal, D. Kuperman, S. Traister, and M. Tur, "The polarization dependence of the RF spectrum in systems having PMD and PDL," in *Proc. ECOC*, Sep. 2003, vol. 3, pp. 534–535.

[15] T. Takahashi, T. Imai, and M. Aiki, "Automatic compensation technique for timewise fluctuating polarisation mode dispersion in in-line amplifier systems," *IEE Electron. Lett.*, vol. 30, pp. 348–349, Feb. 1994.

[16] T. Ono, S. Yamazaki, H. Shimizu, and H. Emura, "Polarization control method for suppressing polarization mode dispersion influence in optical transmission systems," *J. Lightw. Technol.*, vol. 12, no. 5, pp. 891–898, May 1994.

[17] F. Roy, C. Francia, F. Bruyère, and D. Penninckx, "A simple dynamic polarization mode dispersion compensator," in *Proc. OFC*, Feb. 1999, vol. 1, pp. 275–278.

[18] E. Forestieri, "A fast and accurate method for evaluating joint second-order PMD statistics," *IEEE J. Lightw. Technol.*, vol. 21, pp. 2942–2952, Nov. 2003.

[19] D. Yevick, "The accuracy of multicanonical system models," *IEEE Photon. Technol. Lett.*, vol. 15, no. 2, pp. 224–226, Feb. 2003.

[20] S. L. Fogal, W. L. Kath, and G. Biondini, "Multicanonical Monte Carlo simulations of first- and second-order PMD," in *Proc. IEEE LEOS Topical Meeting on PMD*, Jul. 2003, pp. TuB2.2/33–TuB2.2/34.

[21] D. Yevick, "Multicanonical evaluation of joint probability density functions in communication system modeling," *IEEE Photon. Technol. Lett.*, vol. 15, no. 11, pp. 1540–1542, Nov. 2003.

[22] G. J. Foschini, L. E. Nelson, R. M. Jopson, and H. Kogelnik, "Probability densities of second-order polarization mode dispersion including polarization dependent chromatic fiber dispersion," *IEEE Photon. Technol. Lett.*, vol. 12, no. 3, pp. 293–295, Mar. 2000.

[23] T. Lu, D. Yevick, M. O'Sullivan, and M. Reimer, "Multicanonical comparison of polarization-mode dispersion compensator performance," *J. Opt. Soc. Amer. A*, vol. 22, no. 12, pp. 2804–2809, Dec. 2005.

[24] M. Secondini and E. Forestieri, "All-order PMD outage probability evaluation by Markov Chain Monte Carlo simulations," *IEEE Photon. Technol. Lett.*, vol. 17, no. 7, pp. 1417–1419, Jul. 2005.

[25] A. Vannucci, A. Bononi, and L. Gavini, "A new control for double-stage optical PMD compensators and its geometrical interpretation," in *Proc. ECOC*, Sep. 2003, vol. 3, pp. 536–537.

[26] F. Ayres, Jr., *Theory and Problems of Plane and Spherical Trigonometry*. New York: Schaum, 1954.

[27] E. Forestieri, G. Colavolpe, and G. Prati, "Novel MSE adaptive control of optical PMD compensators," *J. Lightw. Technol.*, vol. 20, no. 12, pp. 1997–2003, Dec. 2002.

[28] F. Heismann, D. A. Fishman, and D. L. Wilson, "Automatic compensation of first-order polarization mode dispersion in a 10 Gb/s transmission system," in *Proc. ECOC*, Sep. 1998, vol. 1, pp. 529–530.

[29] M. Shtaif, A. Mecozzi, M. Tur, and J. A. Nagel, "A compensator for the effects of high-order polarization mode dispersion in optical fibers," *IEEE Photon. Technol. Lett.*, vol. 12, no. 4, pp. 434–436, Apr. 2000.

[30] J. J. Hunter, *Mathematical Techniques of Applied Probability*. New York: Academic, 1983.

Armando Vannucci (S'95–M'02) was born in Frosinone, Italy, in 1968. He received the degree in electronics engineering (*cum laude*) from the University of Roma "La Sapienza," Italy, and the Ph.D. degree in information engineering from the University of Parma, Italy, in 1993 and 1998, respectively.

Until 1995, he was with the INFO-COM Department, University of Roma. Since 1995, he has been with the Dipartimento di Ingegneria dell'Informazione, University of Parma, Italy, where he is now an Assistant Professor of telecommunications. His current research interests are in the field of optical communication systems and include polarization mode dispersion, nonlinear WDM fiber transmission, system performance evaluation, and optical amplifiers.

Alberto Bononi received the Laurea degree in electronics engineering (*cum laude*) from the University of Pisa, Italy, in 1988, and the M.A. and Ph.D. degrees in electrical engineering from Princeton University, Princeton, NJ, 1992, and 1994, respectively.

He is an Associate Professor of telecommunications at the School of Engineering, Università di Parma, Italy. He teaches courses in probability theory and stochastic processes, telecommunications networks, and optical communications. In 1990, he was with GEC-Marconi Hirst Research Centre, Wembley, U.K., on a Marconi S.p.A. project on coherent optical systems. From 1994 to 1996, he was an Assistant Professor in the Electrical and Computer Engineering Department, State University of New York (SUNY), Buffalo, teaching courses in electric circuits and optical networks. In the summers of 1997 and 1999, he was a visiting faculty at the Département de Genie électrique, Université Laval, QC, Canada, doing research on fiber amplifiers. His present research interests include system design and performance analysis of high-speed all-optical networks, nonlinear fiber transmission for WDM systems, linear and nonlinear polarization mode dispersion, and transient gain dynamics in optical amplifiers.

Prof. Bononi is currently an Associate Editor of the IEEE TRANSACTIONS ON COMMUNICATIONS for the area of Optical Communications and Networks.